NANOSYSTEMS:
PHYSICS, CHEMISTRY, MATHEMATICS

Sadovnikov S.I. *Nanosystems:*
Phys. Chem. Math., 2026, **17** (1), 90–96.
http://nanojournal.ifmo.ru

Original article

DOI 10.17586/2220-8054-2026-17-1-90-96

Stability of solid-phase heteronanostructures based on zinc and silver sulfides to oxidation

Stanislav I. Sadovnikov

Institute of Solid State Chemistry of the Ural Branch of the Russian Academy of Sciences, Ekaterinburg, Russia

sadovnikov@ihim.uran.ru

PACS 61.46.-w, 61.82.Fk, 65.80.+n, 81.65.Mq

ABSTRACT For the first time the thermal stability of the phase composition of (ZnS)$(Ag_2S)_x$ sulfide heteronanostructures are studied. Solid-phase heteronanostructures (ZnS)$(Ag_2S)_x$ with $x = 0.002 – 0.50$ are synthesized by hydrochemical co-deposition of ZnS and Ag_2S sulfides. The ZnS nanoparticle size, estimated from the broadening of diffraction reflections, in the produced initial heteronanostructures is 2 – 4 nm. Annealing of the synthesized (ZnS)$(Ag_2S)_x$ heteronanostructures in air at temperature from 25 to 530 °C and above leads to a change in their phase composition due to the oxidation of cubic ZnS sulfide to hexagonal zinc oxide. Oxidation begins at a temperature of approximately 250 °C; the ZnO nanoparticle size varies in a range of 12 to 17 – 25 nm. Oxidation of solid-phase (ZnS)$(Ag_2S)_x$ heteronanostructures in air showed that weight loss that occurs upon heating from ∼250 to ∼430 – 450 °C is associated with the beginning of oxidation of the ZnS sulfide and the formation of the ZnO oxide. The most significant weight loss is observed after heating from ∼450 to ∼580 °C due to an increase in the ZnO content, oxidation of sulfur and its removal in the form of SO_2.

KEYWORDS chemical co-deposition, heteronanostructure (ZnS)$(Ag_2S)_x$, stability of phase composition

ACKNOWLEDGEMENTS This study was carried out in accordance with the state assignment No. 124020600013-9 for the Institute of Solid State Chemistry of the Ural Branch of the Russian Academy of Sciences. Author is grateful to Dr. E.Yu. Gerasimov for help in the HAADF-STEM study.

FOR CITATION Sadovnikov S.I. Stability of solid-phase heteronanostructures based on zinc and silver sulfides to oxidation. *Nanosystems: Phys. Chem. Math.*, 2026, **17** (1), 90–96.

1. Introduction

Semiconductor sulfides ZnS and Ag_2S are widely used in various electronic devices, solar cells, light-emitting diodes, luminophores, and catalysts [1–6]. Cubic (space group $F\bar{4}3m$) zinc sulfide α-ZnS is a wide bandgap semiconductor with a band gap of $E_g = 3.50 – 3.76$ eV [4]. Silver sulfide has two main modifications: monoclinic (space group $P2_1/c$) acanthite α-Ag_2S, which exists at temperatures below 180 °C, and body-centered cubic (space group $Im\bar{3}m$) argentite β-Ag_2S, which exists in a temperature range of 180 – 585 °C. The conventional band gap of silver sulfide with α-Ag_2S acanthite structure is 0.9 – 1.1 eV [3].

An increase in the band gap of nanostructured sulfides and heteronanostructures is possible by decreasing the size of nanoparticles and by creating nanocomposites of two sulfides. The most promising is the production of semiconductor nanocomposites consisting of zinc and silver sulfide nanoparticles. In the ideal case, the change in the band gap of the sulfide heteronanostructure of ZnS and Ag_2S can cover a wide part of the spectrum from the infrared to the near ultraviolet. An increase in the Ag_2S content in (ZnS)$(Ag_2S)_x$ heteronanostructures leads to a decrease in the band gap E_g from ∼3.6 – 3.7 to ∼3.0 eV [5]. The use of (ZnS)$(Ag_2S)_x$ heteronanostructures extends the spectral sensitivity to the visible long-wavelength region and allows obtaining new nanomaterials for converting solar energy into electricity, for solid-state UV lasers and fast-acting resistance switches.

The thermal stability of the phase composition of (ZnS)$(Ag_2S)_x$ heteronanostructures is important for their possible application. During the heating of (ZnS)$(Ag_2S)_x$ heteronanostructures, the sulfides can be oxidized. Therefore, for the use of (ZnS)$(Ag_2S)_x$ heteronanostructures, it is necessary to know the stability of their phase composition. There are no published data on the thermal stability of (ZnS)$(Ag_2S)_x$ heteronanostructures. This work is devoted to studying the thermal stability of the composition of (ZnS)$(Ag_2S)_x$ sulfide heteronanostructures containing different relative amounts of silver sulfide x from 0.002 to 0.50.

2. Experimental

Aqueous solutions of reagents for the synthesis of solid-phase heteronanostructures of zinc and silver sulfides were prepared using high-purity deionized water as a solvent.

Synthesis of solid-phase (ZnS)$(Ag_2S)_x$ heteronanostructures by hydrochemical two-stage co-deposition of ZnS and Ag_2S is described in detail earlier in study [5].

Aqueous solutions of reagents for synthesis of ZnS and Ag_2S sulfides and their heteronanostructures based on ZnS and Ag_2S sulfides were prepared with the use of high-purity deionized water as a solvent. High-purity deionized water was produced using the Milli-Q Reference (Merck, Millipore) water preparation system. The specific resistivity of water is equal 18.2 MΩ·cm at 298 K (electrical conductivity is below 5.5×10^{-6} S·m^{-1}), the total content of organic carbon did not exceed 5×10^{10} ppb (5×10^{10} mg·L^{-1}).

The solubility products K_{sp} of sulfides ZnS ($K_{sp} = 2.5 \times 10^{-22}$) and Ag_2S ($K_{sp} = 6.3 \times 10^{-50}$) differ very strongly. Therefore, heteronanostructures ZnS/Ag_2S have been synthesized in two stages. First, silver sulfide Ag_2S was synthesized by chemical deposition from aqueous solutions of silver nitrate $AgNO_3$ and sodium sulfide Na_2S in the presence of sodium citrate Na_3Cit. In aqueous solutions, sodium citrate can reduce Ag^+ ions to form silver metal nanoparticles [3,4] and create a citrate shell on Ag_2S particles [3]. Therefore, to obtain colloidal solutions of silver sulfide without Ag impurities and without a citrate shell, reaction mixtures with a small relative excess of sodium sulfide Na_2S and with Na_3Cit concentration from 0.8 to 10.0 mmol·L^{-1} were used which is lower than the concentration of Na_2S. The synthesis of a colloidal Ag_2S solution was carried out in the dark in a neutral medium at pH $\approx$ 7 according to the following reaction scheme

$$2AgNO_3 + Na_2S \rightarrow Ag_2S\downarrow + 2NaNO_3. \quad (1)$$

For the synthesis of (ZnS)$(Ag_2S)_x$ heteronanostructures, solution of sodium sulfide Na_2S was added to an aqueous zinc nitrate or sulfate solutions under constant stirring and obtained ZnS solution was mixed with synthesized colloidal silver sulfide solution.

The deposition of zinc sulfide occurs by the following reaction scheme

$$Zn(NO_3)_2 + Na_2S \rightarrow ZnS\downarrow + 2NaNO_3. \quad (2)$$

A total of ten (ZnS)$(Ag_2S)_x$ heteronanostructures with relative silver sulfide Ag_2S content x from 0.002 to 0.50 were synthesized. The oxidation of (ZnS)$(Ag_2S)_x$ heteronanostructures with low ($x < 0.025$) silver sulfide content is almost indistinguishable from the oxidation of zinc sulfide. Therefore, in this work, the stability to oxidation of four (ZnS)$(Ag_2S)_x$ heteronanostructures with maximum relative silver sulfide content x from 0.025 to 0.50 is considered in detail. The compositions of the reaction mixtures and composition x of synthesized (ZnS)$(Ag_2S)_x$ heteronanostructures are given in Table 1.

TABLE 1. Composition of reaction mixtures (mmol·L^{-1}), composition x of synthesized (ZnS)$(Ag_2S)_x$ heteronanostructures, and lattice constant a_{B3} of zinc sulfide in the prepared heteronanostructures

No.	Synthesis of ZnS		Synthesis of Ag_2S			Content x in heteronanostructures (ZnS)$(Ag_2S)_x$	a_{B3}, nm
	$Zn(NO_3)_2$	Na_2S	$AgNO_3$	Na_2S	Na_3Cit		
1	50	50	2.5	1.25	0.8	0.025	0.5388
2	50	50	5.0	2.5	2.0	0.05	0.5385
3	50	50	10.0	5.0	4.0	0.10	0.5387
4	50	50	50.0	25.0	10.0	0.50	0.5398

*Lattice parameters of monoclinic (space group $P2_1/c$) acanthite α-Ag_2S, the diffraction reflections of which are observed in the XRD patterns of the synthesized heteronanostructures 3 and 4 are $a = 0.4220$ nm, $b = 0.621$ nm, $c = 0.9531$ nm, and $\beta = 125.43°$.

The $Zn(NO_3)_2$ and Na_2S concentration was 50 mmol·L^{-1} in all reaction mixtures. The synthesized solid-phase powders were washed by decantation and were dried by the sublimation method in an Alpha 1-2 LDplus freeze dryer (Martin Christ) at an ice condenser temperature of -55 °C. Dried sulfide heteronanostructures stored in a Vacuum Desiccator Sanplatec MB, evacuated to a residual pressure of 13.3 Pa (0.1 mm Hg).

The deposited sulfide powders and the same powders after annealing were studied by X-ray diffraction (XRD) on a Shimadzu XRD-7000 diffractometer using Cu$K\alpha_{1,2}$ radiation at room temperature. XRD measurements were performed in the angle interval $2\theta = 20 – 95°$ with a step $\Delta(2\theta) = 0.02°$ at a scanning time of 10 s per point. The determination of the crystal lattice parameters and the final refinement of the structure of the synthesized sulfide powders were carried out using the X'Pert Plus software package [7]. The diffraction reflections of all synthesized nanopowders are significantly broadened due to the small particle size. Nanoparticle size D of ZnS, Ag_2S, and ZnO was determined from the broadening of the diffraction reflections.

The microstructure of the synthesized ZnS/Ag_2S heteronanostructures was studied using a ThemisZ transmission electron microscope (Thermo Fisher, USA) in direct image and in high-angle annular dark-field scanning transmission electron microscopy (HAADF-STEM) mode.

The oxidation of the synthesized heteronanostructures was studied on a Netzsch STA 449C Jupiter thermal analyzer coupled to a QMS 403C Aeolos quadrupole mass spectrometer. The measurements were performed by combined thermogravimetry (TG) and differential scanning calorimetry (DSC) in lidless alundum crucibles under conditions of continuous heating of samples to 700 °C at a rate of 10 °C·min^{-1} in a stream (30 cm^3·min^{-1}) of synthetic air (79 % N_2 + 21 % O_2). Analysis of gases formed during the heating of the samples was carried out taking into account the mass numbers 18, 44, 64 and 80 characteristic of water and CO_2, SO_2, and SO_3 oxides.

3. Results and discussion

The effect of annealing temperature on the evolution of the XRD patterns of heteronanostructures (ZnS)$(Ag_2S)_{0.025}$, (ZnS)$(Ag_2S)_{0.10}$, and (ZnS)$(Ag_2S)_{0.50}$ (see Table 1) containing different amounts of silver sulfide is shown in Figs. 1 and 2, respectively.

Evolution of the XRD patterns of the (ZnS)$(Ag_2S)_{0.025}$ and (ZnS)$(Ag_2S)_{0.10}$ heteronanostructures due to annealing in air at temperatures of up to 380 °C is shown in Fig. 1. Performed quantitative analysis and comparison with the literature

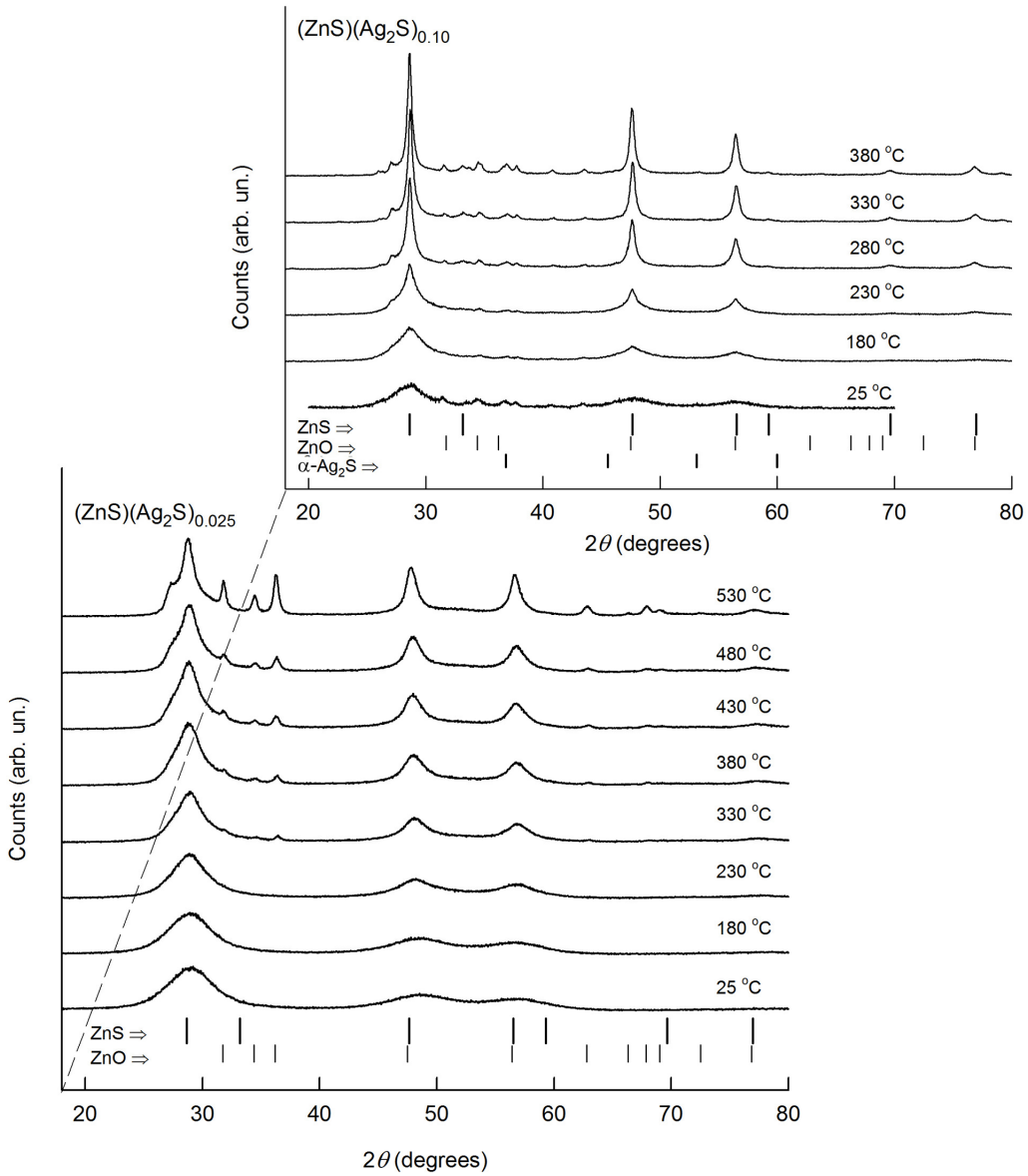

FIG. 1. Effect of an annealing temperature of 25 – 530 °C on XRD patterns of heteronanostructures (ZnS)$(Ag_2S)_{0.025}$ and effect of annealing temperature of 25 – 380 °C on (ZnS)$(Ag_2S)_{0.10}$. Long and medium-length ticks show the positions of reflections of cubic (space group $F\overline{4}3m$) zinc sulfide ZnS and hexagonal (space group $P6_3mc$) zinc oxide ZnO, respectively. Short ticks in bottom of XRD of (ZnS)$(Ag_2S)_{0.10}$ heteronanostructure show the positions of reflections of monoclinic (space group $P2_1/c$) acanthite α-Ag_2S

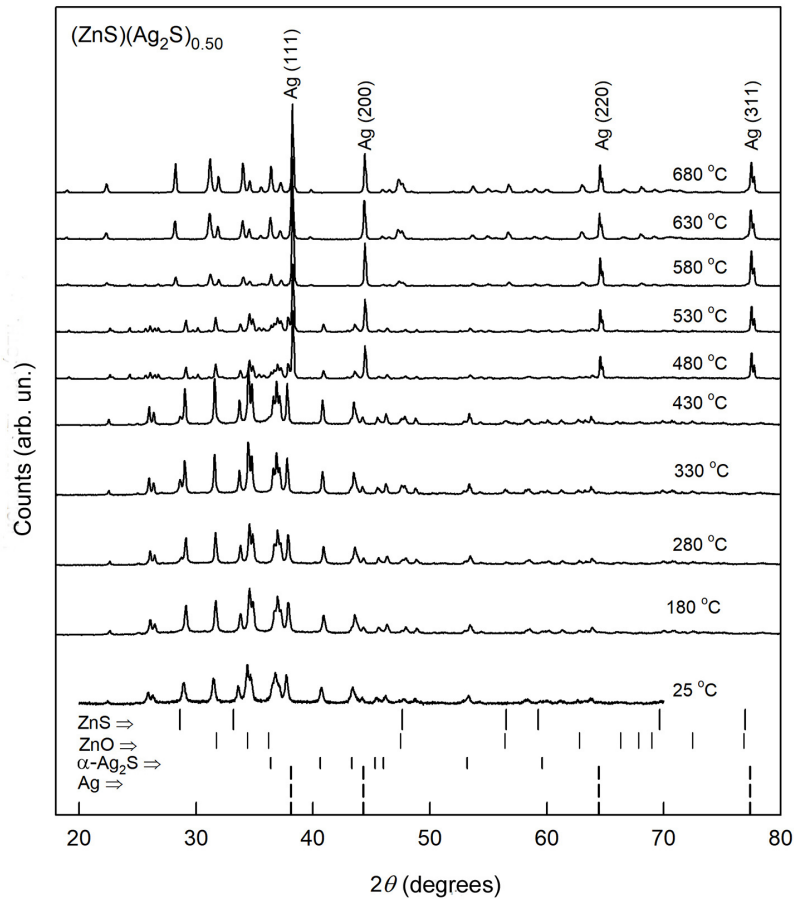

FIG. 2. Evolution of the XRD patterns of heteronanostructure $(ZnS)(Ag_2S)_{0.50}$ due to annealing in air at temperatures from 25 to 680 °C. Long, medium-length, and short ticks show the positions of reflections of cubic zinc sulfide ZnS, hexagonal (space group $P6_3mc$) zinc oxide ZnO, and monoclinic (space group $P2_1/c$) acanthite α-Ag_2S, respectively. The dashed ticks in bottom show the positions of the reflections of the metallic cubic silver Ag.

data showed that the observed sets of diffraction reflections of the initial heteronanostructures at room temperature 25 °C correspond to single-phase cubic (space group $F\overline{4}3m$) sulfide ZnS with a sphalerite structure ($B3$ type). The XRD pattern of the initial heteronanostructures at 25 °C exhibits only highly broadened diffraction reflections of cubic sulfide ZnS. The ZnS nanoparticle size in initial heteronanostructure is ∼3 – 4 nm. The lattice constant a_{B3} of the ZnS nanoparticles is ∼0.5387 nm (Table 1). An increase in the annealing temperature is accompanied by the intensity growth of diffraction reflections due to size increase in the cubic ZnS sulfide particles and the appearance of reflections of hexagonal oxide ZnO. The ZnS nanoparticle size after heating this heteronanostructure in air at 330 and 380 °C is ∼15 – 16 and ∼18 – 24 nm, respectively. In the XRD patterns of the heteronanostructure $(ZnS)(Ag_2S)_{0.10}$ at temperatures up to 380 °C, diffraction reflections of monoclinic silver sulfide (acanthite) α-Ag_2S are also observed. The oxidation of the $(ZnS)(Ag_2S)_{0.025}$ and $(ZnS)(Ag_2S)_{0.10}$ heteronanostructures with the formation of zinc oxide ZnO begins at 280 °C. According to the data of energy-dispersive X-ray analysis, the content of zinc and sulfur in the synthesized heteronanostructures with a mean ZnS nanoparticle size of ∼3 – 4 nm is 50.2±0.1 and 49.9±0.1 at.%, respectively, which corresponds to the stoichiometric ZnS sulfide.

The evolution of the XRD patterns of the $(ZnS)(Ag_2S)_{0.05}$ heteronanostructure upon heating in air is the same as for the $(ZnS)(Ag_2S)_{0.025}$ heteronanostructure. According to the X-ray diffraction data, oxidation of the $(ZnS)(Ag_2S)_{0.05}$ heteronanostructure begins at a temperature 280 °C, when diffraction reflections (100) and (101) of hexagonal zinc oxide ZnO appear.

Changes in the XRD patterns of the $(ZnS)(Ag_2S)_{0.50}$ heteronanostructure due to heating in air at temperatures of up to 680 °C is shown in Fig. 2. Note that XRD patterns of the samples annealed at temperatures of 180 – 680 °C were recorded at room temperature. Due to the high silver sulfide content, the initial heteronanostructure exhibits, along with diffraction reflections of cubic ZnS, diffraction reflections of monoclinic (space group $P2_1/c$) acanthite α-Ag_2S (at 25, 180, 280, 330, 430 °C). Diffraction reflections of body-centered cubic argentite β-Ag_2S, which is equilibrium at a temperature 330 °C and above, are not observed, because the acanthite ↔ argentite transition is reversible. As a consequence, after

cooling the annealed samples, only reflections of monoclinic acanthite, which is an equilibrium low-temperature phase of silver sulfide, are detected.

As in the case of the (ZnS)$(Ag_2S)_{0.025}$ and (ZnS)$(Ag_2S)_{0.10}$ heteronanostructures, oxidation of heteronanostructure (ZnS)$(Ag_2S)_{0.50}$ with the formation of hexagonal (space group $P6_3mc$) zinc oxide ZnO begins at 280 °C too. The size of ZnO nanoparticles in all heteronanostructures during oxidation varies in a range of 12 to 17 – 25 nm. At a temperature of 480 °C and above, due to heating in air, silver sulfide β-Ag_2S decomposes to release cubic metallic silver Ag with a lattice constant $a_{Ag} = 0.4086$ nm (Fig. 2). It is caused by the specific properties of silver sulfide compared with properties of other sulfides. Indeed, Ag_2S does not interact with oxygen during heating in air to a temperature of ∼480 °C. Annealing in air at temperature > 480 °C is accompanied by the decomposition of silver sulfide with releasing metallic silver Ag and sulfur S. Sulfur is oxidized to gaseous sulfur dioxide:

$$Ag_2S + O_2 \rightarrow 2Ag + SO_2 \uparrow . \quad (3)$$

As a consequence, at temperature 480 °C and above, the diffraction reflections of cubic sulfide ZnS, hexagonal oxide ZnO, and cubic silver Ag are observed in the XRD pattern of heteronanostructure (ZnS)$(Ag_2S)_{0.50}$. A similar spontaneous release of Ag in the form of whiskers during heating Ag_2S to 530 – 630 °C was found in [8]. The appearance of Ag whiskers on the surface of a compressed α-Ag_2S tablet heated in air to ∼300 °C was observed in study [9].

Figure 3 shows the TEM image of the (ZnS)$(Ag_2S)_{0.50}$ heteronanostructure in the HAADF-STEM mode and the distribution of the elements Ag, Zn and S in it. The heteronanostructure is a nanocrystalline matrix of zinc sulfide particles doped with silver sulfide nanoparticles. The content of Ag, Zn and S elements in this heteronanostructure is ∼28.5, ∼28.5 and ∼42.9 at.%, respectively.

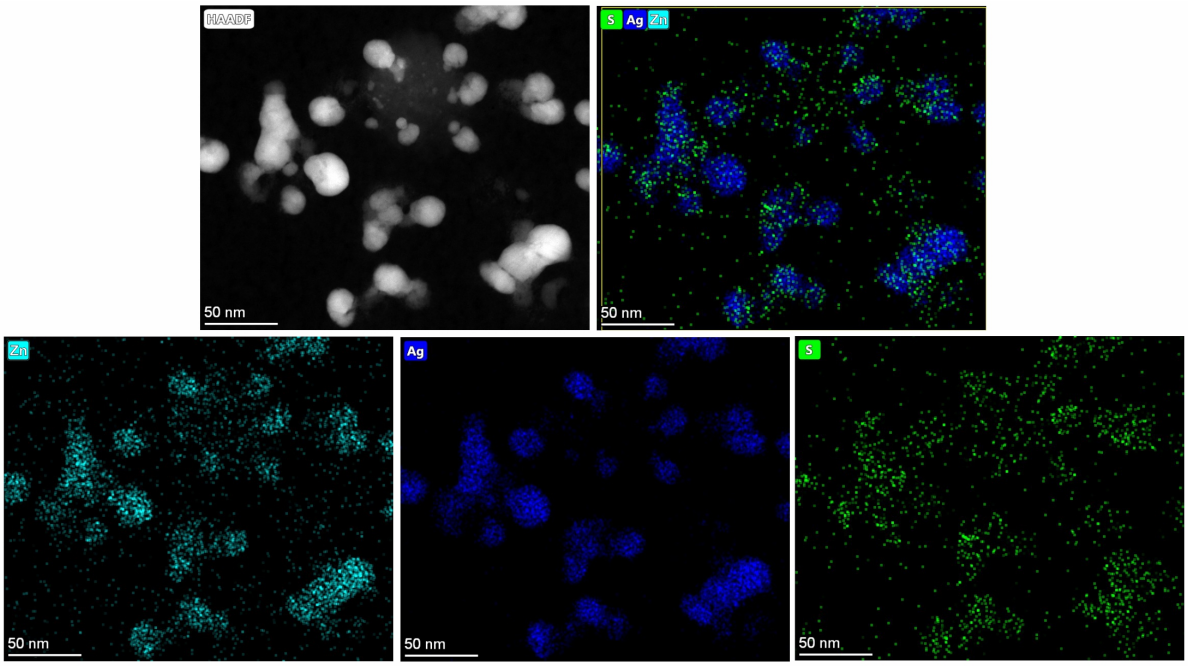

FIG. 3. HAADF image of the initial synthesized heteronanostructure (ZnS)$(Ag_2S)_{0.50}$, HAADF-STEM image of this heteronanostructure with an overlay of EDX distribution maps of S, Zn and Ag, and EDX distribution maps of zinc Zn, silver Ag and sulfur S in this heteronanostructure

From Fig. 3 it is seen that darker silver-containing Ag_2S nanoparticles ∼3 nm in size are predominantly located on the surface lighter ZnS nanoparticles containing zinc. According to X-ray diffraction data, in the initial synthesized (ZnS)$(Ag_2S)_{0.50}$ heteronanostructure, the size of ZnS and Ag_2S nanoparticles is 6 – 7 and 3 – 4 nm, respectively.

Transformations that occur during heating in air and the oxidation of (ZnS)$(Ag_2S)_x$ heteronanostructures were studied by the differential thermal analysis (DTA) – differential thermogravimetry (DTG) method.

Figure 4 shows as an example typical temperature dependences of ion current I_{ion} and DTA-DTG dependences measured during the heating of the (ZnS)$(Ag_2S)_{0.50}$ heteronanostructure in air to 700 °C. An effect associated with the removal of 3 – 4 wt.% of adsorbed water was revealed in the DSC curve at 106 °C. The evaporation of water is confirmed by the presence of a maximum at ∼117 °C in the temperature dependence of ion current for a mass number of 18 corresponding to H_2O [9]. When heating the (ZnS)$(Ag_2S)_{0.50}$ heteronanostructure, the beginning of oxidation is recorded on the DSC curve at 254 °C. It is due to a decrease in the sample mass and the appearance of a small exothermic effect that accompanied by the release of SO_2. This can be explained not only by the partial sublimation of the formed ZnO, but also by the continuation of the ZnS oxidation, which is confirmed by the XRD data. The exothermic effect detected in the

DSC curve at 401 °C corresponds to the release of CO_2 due to the oxidation of the citrate carbon-containing radical to carbon dioxide. The presence of a citrate carbon-containing shell on the surface of heteronanostructures was confirmed earlier in [5]. This is confirmed by the maximum at 388 °C observed in the temperature dependence of ion current for a mass number 44 corresponding to CO_2 (see Fig. 4).

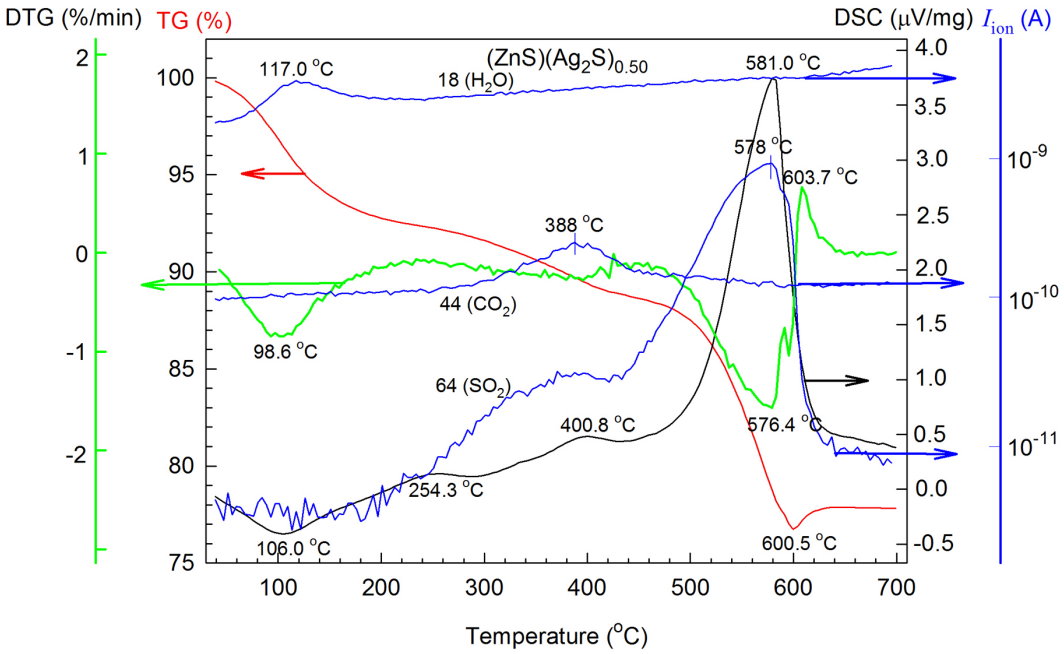

FIG. 4. Differential thermal analysis – DTG dependences measured during the heating of heteronanostructure $(ZnS)(Ag_2S)_{0.50}$ in air and analysis of the evolved gases. Maxima observed in the temperature dependencies of ion current I_{ion} at ∼117, ∼388, and ∼370 – 400 °C are attributed to the release of H_2O steam and CO_2 and SO_2 gases, respectively.

The mass loss occurring upon heating the sample from the beginning oxidation temperature 254 °C to ∼430 – 450 °C is associated with the beginning of ZnS oxidation and the formation of ZnO oxide, which has a lower molecular weight than ZnS. The largest mass loss ∼12 % is observed during heating from ∼500 to ∼580 °C and is due to an increase in the ZnO content and partial oxidation of sulfur, which is removed as gaseous SO_2 dioxide. The exothermic effect on the DSC curve with a maximum at 581 °C correlates with the release of SO_2 into the gas phase and continued oxidation of the heteronanostructure. The release of SO_2 is confirmed by the presence of maxima at ∼400 and ∼578 °C on the temperature dependence of the ion current for the mass number 64 corresponding to SO_2. The partial oxidation of sulfur and its removal in the form of SO_2 were observed earlier during the oxidation of silver sulfide [10, 11] and zinc sulfide nanopowders [12–14].

During oxidation of the $(ZnS)(Ag_2S)_{0.10}$ heteronanostructure in air, the same DTA-DTG dependencies were observed as in the case of the $(ZnS)(Ag_2S)_{0.50}$ heteronanostructure. The beginning of oxidation at 254 °C agrees with the X-ray diffraction data (see Fig. 1) on the oxidation of ZnS with the formation of hexagonal zinc oxide ZnO. The mass loss observed upon heating the sample to ∼420 – 460 °C is due to the appearance of ZnO oxide, which has a lower molecular weight compared to ZnS. The largest mass loss about 11 % is observed after heating from ∼500 to ∼580 °C and is caused by an increase in the ZnO content and partial oxidation of sulfur, which is removed as gaseous dioxide SO_2. The exothermic effect on the DSC curve with a maximum at ∼580 °C correlates with the removing SO_2 into the gas phase, which is confirmed by the presence of maxima at ∼400 and ∼578 °C on the temperature dependence of the ion current for mass number 64, corresponding to SO_2.

4. Conclusion

Heteronanostructures $(ZnS)(Ag_2S)_x$ with different amounts of Ag_2S were synthesized by the hydrochemical co-deposition method. For the first time the thermal stability of the phase composition of $(ZnS)(Ag_2S)_x$ sulfide heteronanostructures has been studied. The annealing of the synthesized $(ZnS)(Ag_2S)_x$ heteronanostructures in air at 25 – 530 °C and above is accompanied by evolution of their phase composition due to the oxidation of cubic zinc sulfide to hexagonal zinc oxide and to an increase in the ZnS nanoparticles size. The oxidation of the heteronanostructures begins at a temperature of 280 – 330 °C; at an annealing temperature 530 °C, the zinc oxide content in heteronanostructures $(ZnS)(Ag_2S)_{0.25}$ and $(ZnS)(Ag_2S)_{0.50}$ achieves ∼26 – 30 wt.%. The ZnO nanoparticle size depends on the composition of the initial

heteronanostructures. At annealing temperatures 380 and 430 °C, it varies from 12 to 17 – 24 nm and from 13 to 25 – 30 nm.

The mass loss observed upon heating to ∼120 °C is caused by the removal of adsorbed water from the samples, which is confirmed by the presence of a maximum in the temperature dependence of the ion current corresponding to H_2O. Studies of the oxidation of the $(ZnS)(Ag_2S)_x$ heteronanostructures in air by the DTA-DTG method have shown that oxidation begins at ∼250 °C. The largest weight loss ∼12 % is observed after heating from ∼450 to ∼580 °C and is caused by increase of the ZnO content, the partial oxidation of sulfur, and its removal in the form of SO_2. This is confirmed by the presence of maxima at ∼400 and ∼578 °C in the temperature dependence of the ion current corresponding to SO_2.

References

[1] Fang X., Zhai T., Gautam U.K., Li L., Wu L., Bando Y., Golberg D. ZnS nanostructures: From synthesis to applications. *Progr. Mater. Sci.*, 2011, **56** (2), P. 175–287.

[2] Wang X., Huang H., Liang B., Liu Z., Chen D., Shen G. ZnS nanostructures: Synthesis, properties, and applications. *Crit. Rev. Solid State Mater. Sci.*, 2013, **38** (1), P. 57–90.

[3] Sadovnikov S.I., Gusev A.I. Recent progress in nanostructured silver sulfide Ag_2S: From synthesis and nonstoichiometry to properties. *J. Mater. Chem. A*, 2017, **5** (34), P. 17676–17704.

[4] Sadovnikov S.I., Rempel A.A., Gusev A.I. Nanostructured silver sulfide: Synthesis of various forms and their applications. *Rus. Chem. Rev.*, 2018, **87** (4), P. 303–327.

[5] Sadovnikov S.I., Ishchenko A.V., Weinstein I.A. Synthesis and optical properties of nanostructured ZnS and heteronanostructures based on zinc and silver sulfides. *J. Alloys Comp.*, 2020, **831**, 154846.

[6] Liang C.H., Terabe K., Hasegawa T., Aono M. Resistance switching of an individual Ag_2S/Ag nanowire heterostructure. *Nanotechnology*, 2007, **18** (48), 485202.

[7] Xu Z., Bando Y., Wang W., Bai X., Golberg D. Real-time *in situ* HRTEM-resolved resistance switching of Ag_2S nanoscale ionic conductor. *ACS Nano*, 2010, **4** (5), P. 2515–2522.

[8] Basu M., Nazir R., Mahala C., Fageria P., Chaudhary S., Gangopadhyay S., Pande S. Ag_2S/Ag heterostructure: a promising electrocatalyst for hydrogen evolution reaction. *Langmuir*, 2017, **33** (13), P. 3178–3186.

[9] Yang W., Zhang L., Hu Y., Zhong Y., Wu H.B., Lou X.W. Microwave-assisted synthesis of porous Ag_2S-Ag hybrid nanotubes with high visible-light photocatalytic activity. *Angew. Chem. Int. Ed.*, 2012, **51** (46), P. 11501–11504.

[10] Kitova S., Eneva J., Panov A., Haefke H. Infrared photography based on vapor-deposited silver sulfide thin films. *J. Imaging Sci. Technol.*, 1994, **38** (5), P. 484–488.

[11] Minami T. Recent progress in superionic conducting glasses. *J. Non-Cryst. Solids*, 1987, **95–96** (1), P. 107–118.

[12] Hull S., Keen D.A., Sivia D.S., Madden P.A., Wilson M. The high-temperature superionic behaviour of Ag_2S. *J. Phys. Condens. Matter*, 2002, **14** (41), L9–L17.

[13] Lim W.P., Zhang Z., Low H.Y., Chin W.S. Preparation of Ag_2S nanocrystals of predictable shape and size, *Angew. Chem. Int. Ed.*, 2004, **43** (42), P. 5685–5689.

[14] Fang X.S., Bando Y., Golberg D. Inorganic semiconductor nanostructures and their field-emission applications. *J. Mater. Chem.*, 2008, **18** (5), P. 509–522.

[15] Zhu Y.C., Bando Y., Xue D.F. Spontaneous growth and luminescence of zinc sulfide nanobelts. *Appl. Phys. Lett.*, 2003, **82** (11), P. 1769–1771.

[16] Fang X.S., Ye C.H., Zhang L.D., Wang Y.H., Wu Y.C. Temperature-controlled catalysis growth of ZnS nanostructures by the evaporation of ZnS nanopowders. *Adv. Funct. Mater.*, 2005, **15** (1), P. 63–68.

[17] X'Pert HighScore Plus. Version 2.2e (2.2.5). ©2009 PANalytical B. V. Almedo, the Netherlands.

[18] Sadovnikov S.I. Effect of elastic properties of nanostructured Ag_2S and ZnS sulfides on interface formation. *Mater. Sci. Semicond. Proc.*, 2022, **148**, 106766.

[19] Corish J., O'Briain C.D. Electrochemically controlled growth and dissolution of silver whiskers. *J. Mater. Sci.*, 1971, **6** (3), P. 252–259.

[20] Živković D., Sokić M., Živković Ž., Manasijević D., Lj. Balanović L., Štrbac N., Ćosović V., Boyanov B. Thermal study and mechanism of Ag_2S oxidation in air. *J. Therm. Anal. Calorim.*, 2013, **111** (2), P. 1173–1176.

[21] Sadovnikov S.I., Gusev A.I. Thermal expansion, heat capacity and phase transformations in nanocrystalline and coarse-crystalline silver sulfide at 290–970 K. *J. Therm. Anal. Calorim.*, 2018, **131** (2), P. 1155–1164.

[22] Fu Q.-S., Xue Y.-Q., Cui Z.-X., Wang M.-F. Study on the size-dependent oxidation reaction kinetics of nanosized zinc sulfide. *J. Nanomater.* (Hindawi), 2014, **2014**, 856489.

[23] Klyushnikov A.M., Pikalov S.M., Gulyaeva R.I. Kinetics of solid-state oxidation of iron, copper and zinc sulfide mixture. *Chim. Techno Acta*, 2023, **10** (2), 202310202.

[24] Sadovnikov S.I., Sergeeva S.V. Thermal stability of nanocrystalline zinc sulfide ZnS. *Rus. J. Inorg. Chem.*, 2023, **68** (4), P. 379–385.

Submitted 2 September 2024; revised 13 November 2024; accepted 4 December 2025

Information about the authors:

Stanislav I. Sadovnikov – Institute of Solid State Chemistry of the Ural Branch of the Russian Academy of Sciences, Pervomaiskaya, 91, Ekaterinburg, 620990, Russia; ORCID 0000-0002-2033-154X; sadovnikov@ihim.uran.ru

Conflict of interest: The author declares that he has no known competing financial interests or personal relationships that could have appeared to influence the work reported in this paper.